Investigations of Particle Size and Number Density in Advanced Energy Systems

C. S. Wang*
Argonne National Laboratory, Argonne, Illinois
and
J. S. Lindner†
Mississippi State University, Mississippi State, Mississippi

In MHD power plants, significant amounts of seed and slag particles are present in the combustion gas. The existence of these particles will significantly affect the performance of MHD components. Therefore, it is essential to be able to measure or predict the spectrum of the particle size and number density. A series of experimental tests has been conducted to measure the particle sizes and number densities of seed and fly-ash particles by using two-color laser transmissometry. The measured values have been compared with the predictions from a theoretical model, and a reasonable qualitative agreement has been obtained between measurement and theory. The present work has demonstrated our ability to measure and predict particle evolution in MHD environments.

Nomenclature

A = cross-sectional area
C = particle number, mass, or volume density
c = constant
c_p = heat capacity
d = diameter
fn = particle size distribution function
H = enthalpy
h = convective heat-transfer coefficient
I = incident radiation
J = nucleation rate
K = agglomeration kernel
k = thermal conductivity
ℓ = effective pathlength
m = mass flow rate or refraction index
N = average number density
Nu = Nusselt number
n = particle size distribution function
Pr = Prandtl number
Q = extinction coefficient
Re = Reynolds number
r = radius or r coordinate
T = temperature or transmittance
u = velocity
x = axial distance or x coordinate
ϵ = emissivity
λ = wavelength
σ = Stefan-Boltzmann constant or Mie extinction cross section
ρ = density
ϕ = stoichiometric ratio
μ = viscosity

Superscripts
m = constant
$\cdot$ = rate
$-$ = averaged
$*$ = critical value

Subscripts
e = extinction
f = fluid
g = gas stream
in = inlet
m = measured or mass
n = number
o = clean gas stream
out = outlet
t = thermocouple
v = volume
w = wall

Introduction

DURING the combustion of pulverized coal in conventional boilers, it has been estimated that about 1% of the mineral inclusions are vaporized.[1] The remaining inorganic species tend to oxidize and fuse together as the char particles are transformed. Particle sizes arising from this latter process typically range between 5 and 75 μm. As the gas stream is cooled in passing to the convective sections of the facility, the vaporized species will grow via homogeneous and heterogeneous nucleation mechanisms. Generally, particle sizes between 0.03 and 1 μm have been observed.[1,2]

In contrast, the extremely high temperatures required in the magnetohydrodynamic (MHD) topping facility will result in increased vaporization of the coal ash during combustion. Consequently, the ultimate concentration of submicricon ash particles formed in the cooler downstream section of the MHD facility will be higher. Depending on combustor operating conditions (such as temperature, equivalency ratio, and residence time), the extent of the initial vaporization of the coal ash has been estimated to be potentially as high as 40%.[3] The introduction of an easily vaporized seed material during combustion will also contribute to the formation of additional submicron particles in the MHD bottoming facility.

As is the case in conventional boilers, the ash particles that do not vaporize during combustion will slag and possibly fuse together to form larger, micron-sized particles. Although most of this slag will be rejected by the MHD slagging combustor, some of the larger slag particles will pass through the downstream components, forming a liquid slag layer on the walls of the topping cycle components and the radiant boiler and con-

Received May 5, 1988; revision received Jan. 1, 1989.

*Technical Staff Member, Magnetohydrodynamics Program.
†Research Scientist II, Magnetohydrodynamic Energy Center.

tributing to the fouling of the steam-cycle convective passes. Some of the liquid slag on the walls of the upstream components may also be re-entrained in the combustion gas as much larger particles. The size distribution and number density of the seed and/or slag particles formed in the MHD process can have a significant impact on the efficiency and durability of MHD components, as is discussed briefly.

The slag layer flowing in the channel is considered beneficial because it provides a protective coating for the generator electrodes.[4] Additionally, since the slag is ionic, a high conductivity level throughout the generator is thought to be maintained. Unfortunately, anionic fly-ash species, whether entrained in the gas stream or flowing on the component surfaces, can interact with the potassium seed cations.[5,6] If the reaction occurs in the gas phase the free electrons in the plasma will be reduced. Also, a moderate fraction of the particles can increase electron scattering. Both of the processes mentioned previously will effectively decrease the generator performance. If the seed/slag reaction occurs at the liquid-gas interface some portion of the seed can be lost.[7-10] The potential seed depletion from these reactions, which theoretically should be less than 5% in the entire facility, may render the process economically unacceptable. Options for minimizing these seed/slag interactions are under consideration.[11,12]

As may be inferred, the slag and seed particles absorb, emit, and scatter thermal radiation because they are electrically conductive. Theoretical studies[13,14] and experimental observations[15] indicate that at high gas temperatures these particles can significantly enhance thermal radiation heat transfer. An assessment has been made[16] of the potential for thermal damage to the radiant boiler back wall due to the high radiant and convective heat transfer resulting from the seed and ash in the high-velocity gas jet exiting the diffuser. Calculations[16] reveal that this particle-laden jet may burn out the back wall because of the highly intensified particle radiation. In an extreme case, the outer surface of the backwall could erode, owing to the high inertial force of the impinging slag particles.

The MHD combustion temperature of about 2800 K results in the production of a much higher concentration of nitric oxide (NO) than that allowed by U.S. Environmental Protection Agency (EPA) regulations. Thus, NO decomposition in the radiant boiler is a key issue in the MHD environmental control strategy. Because the NO decomposition rate is strongly temperature-dependent[17] and the cooling rate of the gas is strongly governed by the seed and slag in the gas (due to the radiation enhancement),[14] the prediction of NO decomposition can be significantly improved if the size and number density of the particles can be accurately measured or calculated. In addition, the possible effects of particle size and number density and NO decomposition and suppression of NO formation have not yet received any attention.

As the particles proceed through the radiant sections of the plant, a portion of the ash particles entering the radiant boiler is deposited on the walls and collected at the bottom of the furnace through a slag tap. The seed principally remains in the vapor phase until the gas temperature is cooled below the dew point. This temperature is normally observed in the platen superheater. Here, the seed vapor can condense on entrained ash particles (heterogeneous nucleation), be deposited on heat-transfer surfaces (vapor condensation), and self-aggregate (homogeneous nucleation).

Condensation of seed and/or deposition of entrained particles on superheater tubes can severely affect heat transfer by thermally insulating the tube surfaces.[18] Possible results of this potentially difficult-to-remove seed/ash fouling include the following: reduced steam temperature; increased flue gas temperature, which shifts the material deposition zone into the reheater section of the component; bridging between tubes; and increased corrosion.

Clearly, the presence of seed and slag particles in the combustion gas passing through MHD components will significantly affect the predictions of heat transfer rates, NO decomposition, potential burnout and erosion of the back wall of the radiant boiler, and fouling deposition in downstream components. These effects are governed mainly by the size, number density, and, to a lesser extent, the chemical composition of the particles. Therefore, it is essential to be able to measure or calculate the particle size and number density.

To this end, we have initially a study of particle characteristics in MHD facilities. A theoretical model[19] that has been developed calculates the evolution of particles from the inception stage. Additionally, average particle diameters and number densities have been measured in an MHD simulation facility using the technique of transmissometry.[20] The initial experimental and theoretical results correspond to the particle evolution of seed and fly-ash particles. Trends in the experimental and theoretical results based on facility operating conditions are in qualitative agreement.

This paper is organized as follows. In the next two sections, the particle evolution model and scattering formalism are briefly described. The experimental measurement section presents details of the instrument, facility characteristics, and test conditions. Results of the experiments and comparisons with the theoretical model are described. Finally, we summarize our findings and consider additional experiments pertinent to the study of ash and seed nucleation.

Theoretical Model of Particle Evolution

The theoretical model of the evolution of seed and slag particles in MHD systems has been developed.[19] This model calculates the rate change in particle size spectrum as a result of homogeneous nucleation, heterogeneous nucleation (or vapor condensation), agglomeration, and convection. This rate change of particle sizes is governed by the population balance equation[19]

$$\frac{1}{A}\frac{\partial}{\partial x}[Aun(r,x)] + \frac{\partial}{\partial r}[\dot{r}n(r,x)] = J\delta(r-r^*) + \int_0^{r/2^{1/3}} K(r_1,r_2)n(r_1,x)n(r_2,x)\frac{r^2}{r_2^2}\,dr_1 - n(r,x)\int_0^{\infty} K(r,r_1)n(r_1,x)\,dr_1 \quad (1)$$

where $r_2 = (r^3 - r_1^3)^{1/3}$ and $n(r,x)$ is the particle size (r) distribution function at each position (x). The first and second terms on the left-hand side of Eq. (1) represent convection of particles and the particle growth rate due to vapor condensation on existing particles, respectively. The first term on the right-hand side represents the rate of particle formation of critical size r^* from vapor phase due to homogeneous nucleation at supersaturation condition; the second term accounts for the formation of particles of radius r due to particle-particle collisions; and the third term represents the disappearance of particles of radius r due to their collision with all other particles in the spectrum. Therefore, this governing equation includes particle interactions with the bulk flowfield, existing vapors in the flow, and other particles.

Expression $K(r, r_1)$ in Eq. (1) is an agglomeration kernel. For the particle sizes in MHD systems, Brownian diffusion is considered the primary mechanism of particle agglomeration. The particle growth rate ($\dot{r}$) is a function of particle size, Knudsen number, partial pressure of the condensing vapor, saturation pressure at particle temperature, vapor diffusivity, and the work function. Homogeneous nucleation is calculated based on the classical nucleation theory, and the critical size of the embryo is computed from the Gibbs-Thomson relationship. The seed/slag vaporization and equilibrium chemistry are also included in the theoretical model.

The details of this complicated theoretical model can be found from Ref. 19. In summary, the evolution of particles from their inception stage can be obtained by solving the population balance equation (containing a term for the homoge-

neous nucleation process). The size distributions of the particles developed in the flowfield are the result of the competition among three processes: the homogeneous nucleation process, forming new particles; the heterogeneous nucleation process, limiting the growth of number density by condensing vapor on existing particles and relieving the supersaturation for self-nucleation; and the particle agglomeration process. The rates of homogeneous nucleation, heterogeneous nucleation (or vapor condensation), and agglomeration, as well as particle growth rate, supersaturation ratio, and number density and size distributions, can be calculated from the model. The average number density and particle size (Sauter mean radius) at each flow location are calculated from the following equations:

$$N(x) = \int_0^\infty n(r,x)\mathrm{d}r \tag{2}$$

$$r_{32}(x) = \int_0^\infty r^3 n(r,x)\mathrm{d}r \Big/ \int_0^\infty r^2 n(r,x)\mathrm{d}r \tag{3}$$

Two-Color Transmissometry

The theoretical framework of two-color transmissometry has been described elsewhere[20,21] and will not be repeated in detail here. In essence, the transmittance T of incident radiation I through a monodisperse (single-sized particle) distribution is given by Beer's law[22]:

$$T(\lambda) = [I(\lambda)/I_o] = \exp(-C_n \ell \sigma_e) \tag{4}$$

where C_n is the particle number density, ℓ is the effective pathlength, and σ_e is the Mie extinction cross section. In the case of dielectric spherical particles, σ_e depends on the incident wavelength λ_o, the particle radius r, and the refractive index m. The Mie cross section is normally expressed in terms of an extinction coefficient Q_e, which is defined as

$$Q_e = \sigma_e/(\pi r^2) \tag{5}$$

The number density in Eq. (4) can be replaced by the mass or volume density

$$C_m = \rho C_v = (\rho 4\pi r^3 C_n)/3 \tag{6}$$

Thus,

$$T = \exp[(-3\ell C_v Q_e r^2)/(4\pi r^3)] \tag{7}$$

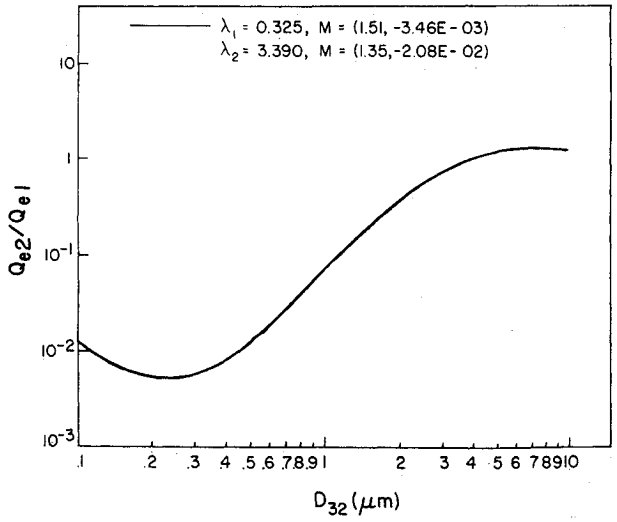

Fig. 1 Mean extinction ratio Q_{e1}/Q_{e2} as a function of particle size D_{32}, wavelength λ, and refractive index M.

Generalization of the preceding equations to polydisperse (different-sized particle) systems is straightforward. All of the parameters that depend on r become average quantities with respect to some form of a distribution; therefore

$$T = \exp[(-3\ell C_v \bar{Q}_e)/(4r_{32})] \tag{8}$$

where the ratio r^3/r^2 has been replaced by the Sauter mean radius,

$$r_{32} = \int_o^\infty r^3 fn(r)\mathrm{d}r \Big/ \int_o^\infty r^2 fn(r)\mathrm{d}r \tag{9}$$

and where $fn(r)$ is a normal-like particle size distribution function while $n(r,x)$ in Eq. (3) needs to be solved numerically and implicitly from Eq. (1). The extinction coefficient can be written as

$$\bar{Q}_e = \bar{\sigma}_e/(\pi \bar{r}^2) = \int_0^\infty \sigma_e fn(r)\mathrm{d}r/\pi \int_0^\infty r^2 fn(r)\mathrm{d}r \tag{10}$$

The expression for $\bar{\sigma}_e$ is the result of a nontrivial calculation[23] and is solved using Ricatti-Bessel and spherical Bessel functions.[24]

The basis of a two-color transmissometer measurement is Eq. (8). Determination of the transmittance of a sample at two distinct wavelengths eliminates dependence on any factors other than those related to the mean extinction coefficients:

$$\ell n T(\lambda_2)/\ell n\ T(\lambda_1) = \bar{Q}_{e2}/\bar{Q}_{e1} \tag{11}$$

The dependence of the ratio $\bar{Q}_{e2}/\bar{Q}_{e1}$ upon the particle size can be displayed as a plot of the ratio as a function of the particle radius or Sauter mean diameter, d_{32}. An example is given in Fig. 1. For this compilation, the distribution function is scaled in equal increments over the d_{32} range of interest while the shape of the distribution is kept constant.

If the measured Q_{e2}/Q_{e1} values correspond to the linear portion of the curve the average particle size can be determined safely. Previous studies have been concerned with the possible errors imposed on d_{32} by different shapes of the assumed distribution and possible variations in the refractive index.[20,25] Current modeling efforts indicate that these errors are small and that d_{32} can be determined to within 0.1 μm by assuming that the coal type or injected material (seed) to the combustor is known.[26] These results are in qualitative agreement with those determined previously.[20,25]

Experimental Measurement

Two-Color Laser Transmissometer

A block diagram of the optical configuration of the microprocessor-controlled transmissometer is given in Fig. 2. The current version of the instrument incorporates three different lasers, although simultaneous measurements at only two wavelengths are necessary to determine the extinction efficiency ratio. Measurements at a different wavelength combi-

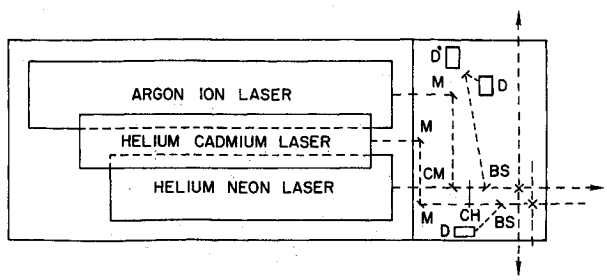

Fig. 2 Diagram of optical configuration of transmissometer; M = flat reflector, CM = coal mirror, CH = chopper, BS = beam splitter, D = low wavelength detector, $D°$ = infrared detector, X = beam director.

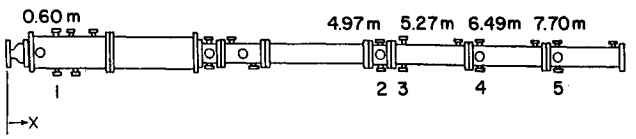

Fig. 3 Test train of the MSU oil-fired MHD simulation facility.

nation such as 0.5145 – 3.39 μm can be used to confirm ratios collected with the 0.325 – 3.39 μm pair. The theoretical response functions, similar to that given in Fig. 1, will have different inflection points corresponding to the measurement wavelengths. The radiation from an argon-ion laser (λ_o = 0.488 or 0.515 μm) with that from a helium-neon laser (λ_o = 3.39 μm) is merged on the cold mirror *CM* and passed through the chopper *CH* operating at 165 Hz. A fraction of the radiation is directed by the beam splitter *BS* to the reference detectors *D* and *D°*. The remaining portion of the beam is reflected from a mirror at point *X* through the optical port. After traversing the gas stream once or twice, the superimposed beams are routed to an additional pair of detectors using another cold mirror. A similar optical component is employed for the reference beams.

Quite recently, a helium-cadmium laser (λ_o = 0.325 μm) has been added to the instrument. In this case, the radiation passes through the unused side of the chopper, and a separate series of optical components and detectors is required. Because of the low power output of the HeCd laser and the moderate particle loadings encountered in this work, the transmission measurements at this wavelength are limited to a single pass.

The signals from the various detectors are amplified and routed to the microprocessor for preliminary evaluation and temporary storage. Commands necessary for specifying the parameters for the data collection routines, as well as general operating protocols, are incorporated in the software and accessed through a hex keypad. Raw intensities from the detectors are displayed on a 20-column printer and stored in the computer memory. When a memory-full condition exists, the entire contents of the buffer are transferred via a general-purpose interface bus (IEEE-488) to a microcomputer. Ultimately, the data are stored on a hard disk for later analysis.

Appropriate software is used to analyze the raw intensities according to Eq. (11). Initially, the dc offset levels are subtracted from the reference and through port detector signals. The intensity through the channel is then normalized to account for possible variations in laser output power. The resulting intensity I is compared with that observed with a clean gas stream I_o and the ratio Q_{e2}/Q_{e1} is determined. The value of Q_{e2}/Q_{e1} is then used to interpolate the appropriate data table (originally calculated on the mainframe computer and stored in the microcomputer software) to find the parameter d_{32} and the corresponding cross sections. Number and/or mass densities, C_n or C_m values, are then calculated from Eqs. (4) and (5). Ultimately, if no trends are observed during a specific operating condition the results for the parameters are averaged.

Test Facility

All of the experiments reported in this work were performed on a simulated MHD test stand.[27,28] The current version of the facility is a 500-kW-throughput oil-fired system capable of a maximum combustion core temperature of 2350 K. Air, at 1.1 atm pressure and a flow rate of 227 kg/h, is preheated to 1100 K by resistance heaters and used to oxidize fuel oil (diesel #1). A primary fuel pump and a peristaltic pump allow the injection of the fuel and K_2SO_4 in slurry, respectively, to the combustor at a maximum rate of 20 kg/h. The remainder of the system consists of the test train (see Fig. 3), slag tap, wet scrubber, and gas exhaust system (not shown). It should be noted that the maximum combustor temperature is sufficient for evaluating the nucleation of K_2SO_4 particles; however, this temperature is too low for studying the corresponding nucleation of fly-ash. Further modifications to the existing test train

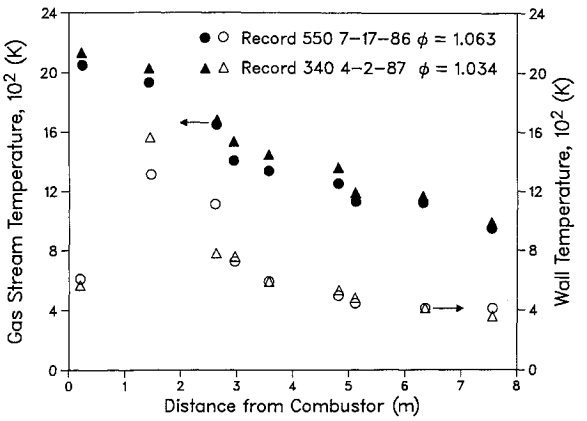

Fig. 4 Measured gas stream (solid symbols) and wall (hollow symbols) temperatures along the test train.

or measurements at other facilities will be required in order to investigate the evolution of fly-ash particles.

The test train is composed of water-cooled, 0.2-m-inside-diameter (ID) piping of various lengths. Sections near the combustor have been packed with refractory; at those locations at which the transmissometer was positioned (ports 3, 4, and 5), the pipe is unaltered. Water cooling for the channel is accomplished using a pump with a 100-hp motor, two sets of fluid coolers, and a 1.14-m^3 water tank.

The test sections are equipped with optical ports, located at specified distances, consisting of a 0.05-m gate valve shutter mounted on 0.05- or 0.078-m-ID pipe, which is welded to the test section. The gate valve can be remotely operated. A 0.078-m-ID pipe is mounted on the outer flange of each valve and provided with a nitrogen purge and a mount for a quartz window (0.025 m thick by 0.1-m diameter). In this work, particular attention was given to the cleanliness of the windows. Particle deposition on the windows will lead to decreased transmissions, which in turn lead to inaccurate determination of gas stream particle diameters.

The entire facility is instrumented with an array of flowmeters, thermocouples, pressure regulators, and other measuring devices. System control and monitoring is achieved through the use of an HP 1000 computer configured to have 125 analog and 16 differential inputs. Equivalency ratios and feed rates can be varied using the control software.

Typical gas and wall temperature profiles along the test train are given in Fig. 4. Gas stream temperatures were measured on the basis of a *Pt/Rh* thermocouple inserted in the gas stream 7.55 m from the combustor. Measured temperatures T_m were corrected to gas stream temperatures T_g by equating the convective and radiative heat transfers of the thermocouple

$$h(T_g - T_m) = \sigma\epsilon_T(T_m^4 - T_w^4) \tag{12}$$

or

$$T_g = T_m + \frac{\sigma\epsilon_t}{h}(T_m^4 - T_w^4) \tag{13}$$

where T_w is the wall temperature, σ is the Stefan-Boltzmann constant, ϵ_t is the emissivity of the thermocouple,[29] and h is the convective heat transfer coefficient. This last quantity is calculated from the Nusselt number Nu:

$$h = Nu\ k/d_t \tag{14}$$

The Nusselt number, in turn, is related to the Reynolds and Prandtl numbers:

$$Nu = cRe^m Pr^{0.33} \tag{15}$$

where

$$Re = \rho u\ d_t/\mu \tag{16}$$

and

$$Pr = \mu\, c_p/\mathrm{k} \tag{17}$$

where ρ is the gas density, u is the velocity, d_t is the diameter of the thermocouple, and μ is the viscosity. The quantities k and c_p are the gas thermal conductivity and heat capacity, respectively. In order to calculate the gas temperature at the beginning of the test section, an energy balance is established on each section to relate the heat lost by the gas phase to the heat gained by the cooling fluid:

$$\dot{m}_g(H_{\text{in}} - H_{\text{out}}) = \dot{m}_f\, c_{pf}(T_{f,\text{out}} - T_{f,\text{in}}) \tag{18}$$

where $\dot{m}_g$ and $\dot{m}_f$ are the mass flow rates of the gas stream and fluid, H is the enthalpy at the entrance and exit of the section, c_{pf} is the heat capacity of the fluid, and T_f signifies the fluid temperatures. Equation (18) is solved for H_{in}, which is then related to the inlet gas stream temperature. This latter temperature is then used as the exit temperature from the next upstream section and the process is repeated. The temperature profile of the test stand is calculated in reverse.

The gas stream temperatures at the port locations investigated with the transmissometer are below the lower limit of the sodium line reversal technique.[28] The proximity of the instrument location to the thermocouple, however, implies that the necessary input gas stream temperatures required for the nucleation model are relatively accurate.

Test Conditions

Several tests have been performed under a wide range of test conditions. The nominal conditions of these tests are summarized in Table 1. The average particle sizes and number densities of the seed particles have been measured at view port numbers 3, 4, and 5 (see Fig. 3). Note that the ranges of the gas and wall temperatures listed in Table 1 represent the temperatures from the inlet (combustor) to the outlet test train. Typical gas and wall temperature profiles along the length of the test train have been plotted in Fig. 4. These typical gas and wall temperatures measured at view port numbers 3, 4, and 5 can be obtained from Fig. 4. During the tests, a sodium line reversal (SLR) instrument was used to measure the gas temperature at an upstream location (view port number 1). The results of the SLR measurements agree with those of the bare thermocouple measurements.

Table 1 Nominal conditions of particle evolution test

Parameter	Value
Combustion feed rates, kg/h	
Air	220–235
No. 1 Diesel Oil	12–17
K_2S0_4	2.1–2.7
Fly ash[a]	0.3–1.4
Stoichiometric ratio, ϕ	0.875–1.230
Temperature, K	
Gas in test train	2250–810
Wall	1680–350
Air preheat	965–990

[a]Montana Rosebud ash with initial size of 6 μm was used.

Results and Discussion

The model calculations of homogeneous nucleation and growth rate are very sensitive to the gas cooling rate and the surface tension of the nucleated droplets.[19] In the present study, the wall and gas temperatures directly measured from the test section were used as inputs for the theoretical calculations. The cooling rates were maintained almost constant during the tests. Because the surface tension of seed droplets has not been reported in the literature, the calculated results shown in this paper were obtained by using the surface tension of the bulk liquid. Montana Rosebud ash with average initial size of 6 μm was used. Other input parameters to the model calculations included system pressure, seed and fly-ash mass flow rates, air and fuel mass flow rates, and the dimensions of the test train.

Table 2 compares the measured and calculated values of average particle sizes and number densities for the tests performed at MSU over a wide range of test conditions (see Table 1). Both the measured and calculated results shown in Table 2 resulted from averaging the data from each test period, and these results are for seed (K_2S0_4) particles only and for seed/fly-ash particles. Some values show very good agreement in the measured and calculated results for both particle size and number density; other comparisons show up to an order of magnitude difference in the number density and a maximum of about 1-μm difference in particle size. A main reason for this disparity in calculated and measured number densities is thought to reside in the fact that the particle number density changes quite rapidly during the nucleation process. For the gas stream temperatures encountered in this study, the onset of particle evolution is confined to upstream locations. The deter-

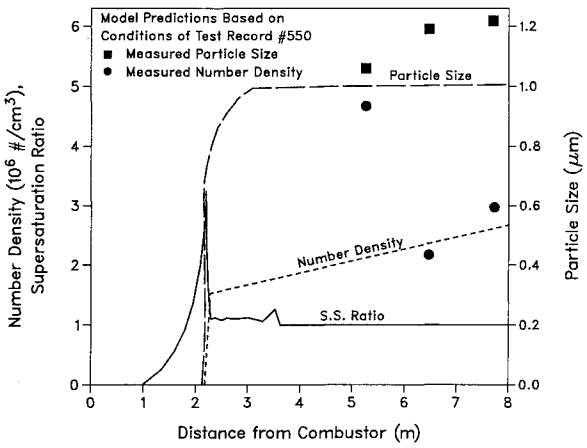

Fig. 5 Model predictions and their comparison with measured values.

Table 2 Comparison between calculated and measured average particle size and number density

Distance from combustor, m	Seed/ash mass flow rates, Kg/h	Stoichiometric ratio	$d_{32}(\mu\text{m})$		C_n 10^6 particles/cm^3	
			Measured	Calculated	Measured	Calculated
5.270	2.27/0.0	1.07	1.06 ± 0.14	1.20	4.66 ± 2.0	2.07
	2.22/0.0	1.03	0.87 ± 0.14	1.50	9.10 ± 2.3	0.92
	2.37/0.0	1.15	0.86 ± 0.15	1.47	7.85 ± 2.6	1.01
	2.22/0.0	1.23	0.87 ± 0.16	1.14	4.10 ± 1.6	1.34
	2.66/0.0	0.88	0.91 ± 0.14	0.99	5.83 ± 2.2	3.87
	2.32/0.32	1.03	1.02 ± 0.22	1.75	5.60 ± 2.0	0.91
	2.42/0.66	1.04	1.20 ± 0.20	1.93	3.90 ± 1.0	0.80
	2.45/1.34	1.03	1.67 ± 0.13	2.60	1.24 ± 0.5	0.47
6.485	2.17/0.0	1.05	1.19 ± 0.14	1.22	2.35 ± 0.6	2.06
7.704	2.13/0.0	1.05	1.22 ± 0.16	1.21	2.93 ± 1.0	2.43

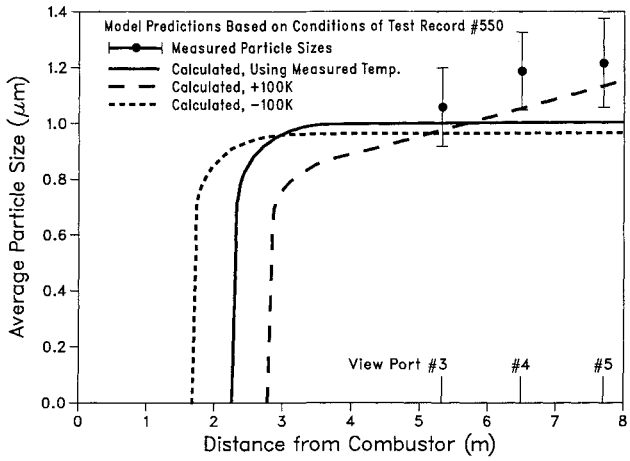

Fig. 6 Effect of gas temperature profiles on particle size predictions.

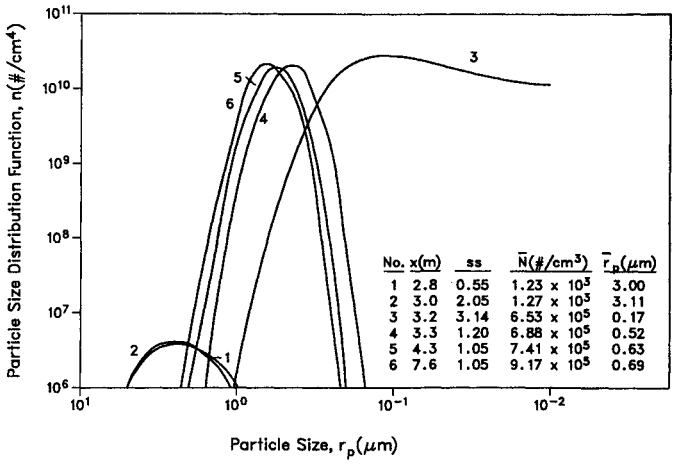

Fig. 7 Typical calculated particles size distribution function along the test train for one of the experiments.

mination of the particle number density is very sensitive to the nucleation process; therefore, the difference between the measured and calculated number densities is larger at locations closer to the initial nucleation zone. At downstream locations, the nucleation process is almost complete; consequently, the measured and calculated number densities and particle sizes are in better agreement. Considering, however, the complexity of the particle evolution processes involved in the computer model and the processes involved in data reduction from the experimental measurements, the comparisons between the measured and calculated values in Table 2 exhibit reasonable qualitative agreement. In Table 2 both the measured and calculated data also show that the stoichiometric ratio does not have a significant effect on particle size and number density.

Figure 5 shows the model predictions of average particle size, number density, and supersaturation ratio of the seed material along the test train for one of the tests for seed particle only. Also shown in Fig. 5 are the measured average values of particle size and number density at the three measurement locations. Note that these measured values at different locations were based on three separated measurements (see Table 2 for seed flow rates of 2.66, 2.17, and 2.13 Kg/h) while the calculated values were based on one of the measured conditions (Record #550 for seed flow rate of 2.66 Kg/h at View Port #3). The supersaturation ratio is defined as the ratio of partial pressure of the seed vapor to its saturation pressure. Theoretically, if this supersaturation ratio is higher than one, the homogeneous nucleation process starts. This figure indicates that the seed vapor starts to form a large number of particles at a supersaturation ratio of about 3. Note that the supersaturation ratio increases and subsequently decreases very rapidly over a very short distance, in which homogeneous nucleation is initiated. The increase in number density along the test train at downstream locations indicates additional homogeneous nucleation as the gas continues to cool.

Figure 6 shows the sensitivity of the gas temperature profile used in model calculations[15] on the particle size predictions. The solid line in Fig. 6 represents the average particle size along the test train (see Fig. 3), calculated by using the measured gas and wall temperature profiles of Record #550's test condition as inputs for the model calculations. With the wall temperature profile unchanged, the dotted and broken lines in Fig. 6 represent the calculated average particle sizes that result from decreasing (−) and increasing (+) by 100 K the measured gas temperature profiles, respectively, as inputs for the model predictions. As expected, this sensitivity study indicates that the higher the gas temperature profile used, the further the distance along the test train before homogeneous nucleation occurs. It also shows that the higher the assumed temperature profile used, the larger the predicted particle size at the downstream locations. This may be due to the reduced vapor condensation on the wall surfaces because of the relatively higher gas temperature; this vapor can then condense on the existing nucleated particles by heterogeneous nucleation at downstream locations. At the two lower gas temperature profiles used in the model calculations the calculated average particle sizes remained constant at downstream locations, and the average particle sizes are smaller than those calculated at the highest temperature profile. This may be due to increased vapor condensation on the wall surface of the test train at the lower gas temperatures. With respect to particle growth, this sensitivity study shows that if the measured gas temperatures are within ± 100 K of the actual values, the model predictions of particle sizes and number densities are still within an acceptable range.

Figure 7 shows the calculated particle size distribution function n along the test train for one of the experiments. This figure indicates that at $x < 3$ m (curves 1 and 2) the particle size distribution corresponded to the size distribution of the fly ash in the slurry fuel. (Note: the fly ash is not vaporized during the combustion in the present experimental system.) At values of $x > 3$ m, the model predicts the homogeneous nucleation of small seed particles and a shift in the particle size distribution curve to very small particles (curve 3). At downstream locations (curves 4, 5, and 6) the peaks of the distribution curves shift to larger particle sizes due to agglomeration and vapor condensation on existing particles. The normal-like particle size distribution functions $n(r,x)$ have been calculated at downstream locations consistent with $fn(r)$ used in the measurements. This may also explain why a better agreement in measured and calculated number density and particle size is obtained with increasing distance from the combustor.

Although additional experiments and calculations are needed, the good agreement between theory and experiment is encouraging. In the future, more tests will be performed with particle size measurements at different cooling rates and different locations along the test train, in particular, at those locations where the calculated particle size is rapidly changing. Ultimately, comparisons of the model predictions with transmissometry measurements will be performed on a large-scale coal-fired facility.

Conclusions

Particle evolution in MHD systems has been theoretically and experimentally studied. A series of experimental tests have been conducted to measure the average particle sizes and number densities of seed and fly-ash particles by using two-color laser transmissometry. The measured values have been compared with theoretical predictions. A reasonable qualitative agreement has been obtained between measurement and theory.

The measured gas and wall temperature profiles along the test train have a significant effect on the predictions of particle nucleation, especially for the inception stage. The higher gas temperature profile will delay the nucleation to further downstream locations. With respect to the particle growth, the calculations show that even if the measured gas temperatures are within ± 100 K of the actual values, the predictions of particle size and number density are still within an acceptable range.

The present study has demonstrated our ability to measure and predict the particle evolution in MHD environments. More theoretical and experimental studies are needed for both seed and slag particles. These studies should include the effects of gas cooling rate, the surface tension of droplets, the measurement of vapor condensation on the wall surfaces, and the presence of vaporized or partially vaporized slag particles in the gas stream.

Acknowledgments

This work was supported by the U.S. Department of Energy, Magnetohydrodynamics Program, under Contracts W-31-109-Eng-38 and DE-AC02-80ET-15601. We acknowledge R. Arun Kumar and J. Luthe for technical support regarding the Mississippi State University test stand and scattering calculations, respectively.

References

[1]Flagen, R. C. and Taylor, D. D., "Laboratory Studies of Submicron Particles from Coal Combustion," *Proceedings of the 18th Symposium (International) on Combustion*, The Combustion Institute, Pittsburgh, PA, 1980, p. 1227.

[2]Ramsden, A. R., "A Microscopic Investigation into the Formation of Flyash during the Combustion of a Pulverized Bituminous Coal," *Journal of the Institute of Fuel*, Vol. 41, No. 451, 1986.

[3]Shuck, R., "Kinetics of Char Burnout and Ash Vaporization in Coal Fired MHD Combustors," *Proceedings of the 18th Symposium on Engineering Aspects of MHD*, Butte, MT, 1979, p. K.1.1.

[4]Carlson, L. W., Zitzow, U., and Rabkin, Y. L. *Open Cycle Magnetohydrodynamic Electrical Power Generation,* edited by M. Petrick and B. Y. Shumyatsky, Argonne National Laboratory, Argonne, IL, 1978, p. 473.

[5]Spencer, F. E., Hendric, J. C., and Bienstock, D., "Equilibrium Electron Density of Coal-Combustion Mixtures – Computer Study and Comparison with Experiment," *Proceedings of the 13th Symposium on Engineering Aspects of MHD*, Stanford University, Stanford, CA, 1973, p. VII-4.

[6]Yousefian, Y., et al., "Computer Modelling of the Effects of Coal Ash Chemistry on the Performance of MHD Generators," *Proceedings of the 18th Symposium on Engineering Aspects of MHD*, Butte, MT, 1979, p. C.4.1.

[7]Luongo, C. A., and Krugar, C. H., "Slag Composition Calculations using a Non-Ideal Solution Model," *Proceedings of the 20th Symposium on Engineering Aspects of MHD*, University of California, Irvine, CA, 1982, p. 12.2.1.

[8]Spencer, F. E., Hendric, J. C., and Bienstock, D., "A Ternary Margules-Type Model for Plasma-Slag Equilibrium in Potassium Seeded Coal Combustion for MHD Power Generation," *Proceedings of the 6th International Conference on MHD Electrical Power Generation,* Vol. II, 1975, p. 181.

[9]Crawford, L. H., et al., "Investigation of Slag Deposits and Seed Absorption in a Direct Fired MHD Power Generator," *Proceedings of the 6th International Conference on MHD Electrical Power Generation*, Vol. II, 1975, p. 51.

[10]Jackson, D. M., "Status of Slag/Seed Interaction Testing at the Coal Fired Flow Facility," *Proceedings of the 22nd Symposium on Engineering Aspects of MHD*, MHD Energy Center, Mississippi State University, Mississippi State, MS, 1984, p. 11.1.1.

[11]Bauer, J. M., and Iwata, H., "Development of Slagging Coal Combustors for MHD," *Proceedings of the 19th Symposium on Engineering Aspects of MHD,* UTSI, Tullahoma, TN, 1981, p. 16.1.1.

[12]Arunachalam, S. A., Rao, G. V. S., and Iyer, D., "Behavior of Coal Particles in MHD Combustors – A Model," *Proceedings of the 23rd Symposium on Engineering Aspects of MHD*, Somerset, PA, 1985, p. 134.

[13]Im, K. H., Ahluwalia, R. K., and Berry, G. F., "Heat Transfer in Slagging MHD Radiant Boilers," AIAA Paper 81-0316, 1981.

[14]Wang, C. S. and Chow, L. S. H., "Thermal Radiation in MHD Design Applications," *Proceedings of the 24th Symposium on Engineering Aspects of MHD,* Butte, MT, 1986, p. 202.

[15]Chow, L. S. H., Smyk, E. B., and Johnson, T. R., "Comparison between Experimental Results and Analytical Predictions of Seed-Slag Fouling in an MHD Steam Bottoming Plant," CONF-83-0634, Argonne National Laboratory, Argonne, IL, 1983.

[16]Berry, G. F., Wang, C. S., and Choi, U. S., "The Effects of Impinging Particle-Laden Gas Jets on the Potential for Burnout in an MHD Radiant Boiler," *Proceedings of the 24th Symposium on Engineering Aspects of MHD,* Butte, MT, 1986, pp. 167–174.

[17]Pepper, J. W. and Krugar, C. H., "Accurate Modeling of NO Decomposition in MHD Steam Power Plant Systems," *Proceedings of the 13th Symposium on Engineering Aspects of MHD,* 1973.

[18]Carlson, L. W., Zitzow, U., and Rabkin, Y. L., *Open Cycle Magnetohdrodynamic Electrical Power Generation*, edited by M. Petrick and B. Y. Shumyatsky, Argonne National Laboratory, Argonne, IL, 1978.

[19]Im, K. H. and Ahluwalia, R. K., "Nucleation of Slag and Seed in MHD Plants," *Proceedings of the 20th Symposium on Engineering Aspects of MHD*, University of California, Irvine, CA, 1982.

[20]Ariessohn, P. C., "Optical Diagnostic Measurements of Coal Slag Parameters in Combustion MHD Systems," HTGL Rept. 119, Stanford University, Stanford, CA, 1980.

[21]Luthe, J. C., and Strickel, R. E., "Two Color Transmissometer," MHD Quarterly Technical Progress Rept. FE-15601-3, *Testing and Evaluation of Heat Recovery/Seed Recovery*, Mississippi State University, Mississippi State, MS, 1980.

[22]van de Hulst, H. C., *Light Scattering by Small Particles*, Dover Publications, New York, 1981.

[23]Born, M. and Wolf, E., *Principles of Optics,* Pergamon Press, New York, 1975.

[24]Abramowitz, M. and Stegun, I. (eds.), *Handbook of Mathematical Functions,* Dover Press, New York, 1965.

[25]Dobbins, R. A. and Jizmagian, G. S., "Particle Size Measurements Based on Use of Mean Scattering Cross Sections," *Journal of Optical Science of Americ*a, Vol. 56, No. 10, 1966.

[26]Lindner, J. S. and Luthe, J. C., "Two Color Laser Transmissometer," Diagnostic Development and Support of MHD Test Facilities Quarterly Technical Progress Rept. FE-15601-25, 1986.

[27]Murphree, D. L., "Remote Sensing of Coal-Fired MHD by Optical Diagnostic Techniques," AIAA Paper 83-0469, 1983.

[28]Cook, R. L. and Murphree, D. L., "Diagnostic Instrumentation Development Program for Testing and Evaluation of Magnetohydrodynamic/Heat Recovery Seed Recovery Components," *Proceedings of the Specialists Meeting on Coal Fired MHD Power Generation*, Sydney, Australia, Aug. 1981.

[29]Kumar, R. personal communication, 1987.